Some Cerium β-Diketonate Derivatives as MOCVD Precursors

Michael Becht, Tobias Gerfin, and Klaus-Hermann Dahmen*

Laboratorium für Anorganische Chemie, ETH Zürich, Universitätsstrasse 6, 8092 Zürich, Switzerland

Received February 21, 1992. Revised Manuscript Received November 16, 1992

Four β-diketonato complexes of cerium were synthesized and investigated by thermal analysis, mass spectrometry, and infrared spectroscopy with respect to their ability to function as possible precursors for MOCVD. Thermal analysis revealed sufficient volatility for all these compounds and an enhancement of the volatility by using fluorinated ligands could be observed. Using all these precursors, growth experiments of cerium dioxide films were carried out in a horizontal MOCVD reactor. The growth rates were determined by ellipsometry and independently by profilometry. The dependence of the growth rate on evaporation rate, oxygen flow and substrate temperature are discussed in detail. Single-phase CeO_2 films with high preferential orientation in the [100] and [111] directions could be prepared on Si[100] and quartz as was shown by X-ray diffraction.

Introduction

Cerium dioxide has long been considered as a useful material for optical coatings due to its high refractive index.[1] However, these films have never found wide application because of a microstructure that is not easily reproducible.[2] The films grow in columns with a typical diameter of several tens of nanometers.[3,4] Nevertheless, in the past 2 years cerium dioxide was investigated as an insulating and chemically stable material for silicon on insulator (SOI) structures[5,6] and for buffer layers. The buffer layers were used for the growth of $YBa_2Cu_3O_{7-\gamma}$ superconducting thin films on silicon[7-9] and $LaAlO_3$.[10] The high-T_c superconducting films prepared on these substrates showed high crystallinity with *a* or *c* axis preferential orientation, high T_c's, and high critical current densities.

It was possible to grow oriented CeO_2 films by electron beam evaporation,[5,6,8] laser ablation,[7,9,10] or spray-ICP technique[11] on Si[100], Si[111], $LaAlO_3$[100], quartz, or sapphire. High-quality CeO_2 films with a [100], [110], or [111] preferential orientation were prepared using these methods.

Cerium dioxide films were also grown by chemical vapor deposition (CVD) using chloride precursors by Taylor et al.[12] A slightly preferential orientation of CeO_2[100] on Si was found, but it was concluded that metal-organic chemical vapor deposition (MOCVD) should improve the growth of films of this oxide. We have previously reported the growth of such films by MOCVD using tetrakis[2,2,6,6-tetramethyl-3,5-heptanedionato]cerium, $Ce(thd)_4$, as precursor.[13,14] It was found that for substrate temperatures above 450 °C the growth rate of the films decreases with increasing temperature. For this reason the thermal stability of the precursor seemed to be low. Addition of ammonia or isopropanol to the carrier gas was not beneficial. However, in the case of H(thd) as stabilizer in the gas phase high growth rates above 500 °C were obtained.

The compounds investigated in this work are the homoleptic tetravalent compounds (A) $Ce(thd)_4$ and tetrakis[6,6,6-trifluoro-2,2-dimethyl-3,5-hexanedionato]-cerium ($Ce(fdh)_4$) and the hetroleptic trivalent compounds (B) 1,10-phenanthrolinetris[2,2,6,6-tetramethyl-3,5-heptanedionato]cerium ($Ce(thd)_3phen$) and 1,10-phenanthrolinetris[6,6,6-trifluoro-2,2-dimethyl-3,5-hexanedionato]-cerium ($Ce(fdh)_3phen$).

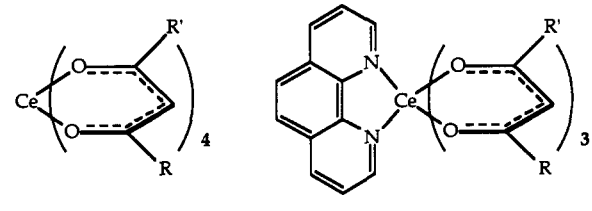

A B

A: $Ce(thd)_4$ R, R' = $(CH_3)_3$; $Ce(fdh)_4$ R = $(CH_3)_3$; R' = CF_3

B: $Ce(thd)_3phen$ R, R' = $(CH_3)_3$, $Ce(fdh)_3phen$ R = $(CH_3)_3$, R' = CF_3

The synthesis of these complexes was published first in 1971, but no spectroscopic data are given.[15] Here, we report

(1) Hass, G.; Ramsey, J. B.; Thun, R. *J. Opt. Soc. Am.* **1958**, *48*, 324.
(2) Netterfield, R. P.; Sainty, W. G.; Martin, P. J.; Sie, S. H. *Appl. Opt.* **1985**, *24*, 2267.
(3) Pearson, J. M. *Thin Solid Films* **1970**, *6*, 349.
(4) Guenther, K. H.; Pulker, H. K. *Appl. Opt.* **1976**, *15*, 2992.
(5) Inoue, T.; Osonoe, M.; Tohda, H.; Hiramatsu, M.; Yamamoto, Y.; Yamanaka, A.; Nakayama, T. *Rep. Res. Ion Beam Technol.* **1990**, *9*, 59.
(6) Inoue, T.; Yamamoto, Y.; Koyama, S.; Suzuki, S.; Ueda, Y. *Appl. Phys. Lett.* **1990**, *56*, 1332.
(7) Yoshimoto, M.; Nagata, H.; Tsukahara, T.; Koinuma, H. *Jpn. J. Appl. Phys., Part 2* **1990**, *29*, L1199.
(8) Nagata, N.; Tsukahara, T.; Gonda, S.; Yoshimoto, M.; Koinuma, H. *Jpn. J. Appl. Phys. Part 2*, **1991**, *30*, L1136.
(9) Luo, L.; Wu, X. D.; Dye, R. C.; Muenchausen, R. E.; Foltyn, S. R.; Coulter, Y.; Maggiore, C. J.; Inoue, T. *Appl. Phys. Lett.* **1991**, *59*, 2043.
(10) Wu, X. D.; Dye, R. C.; Muenchausen, R. E.; Foltyn, S. R.; Maley, M.; Rollett, A. D.; Garcia, A. R.; Nogar, N. S. *Appl. Phys. Lett.* **1991**, *58*, 2165.
(11) Suzuki, M.; Kagawa, M.; Syono, Y.; Hirai, T. *J. Cryst. Growth* **1991**, *112*, 621.
(12) Taylor, H. L.; Trotter, J. D. *Proc. Int. Conf. Chem. Vap. Deposition, 3rd* **1972**, 475.
(13) Dahmen, K.-H.; Becht, M.; Gerfin, T. *High T_c Superconductor Thin Films/* Correra, L., Ed.; Elsevier: Amsterdam, 1992; p 715.
(14) Gerfin, T.; Becht, M.; Dahmen, K.-H. *Ber. Bunsenges. Phys. Chem.* **1991**, *95*, 1565.
(15) Uhlemann, E.; Dietze, F. Z. *Anorg. Allg. Chem.* **1971**, *386*, 329.

0897-4756/93/2805-0137$04.00/0

additional information about the synthesis and the results of mass spectrometry, thermal analysis, and infrared spectroscopy. Carrying out growth experiments with these four precursors, it was possible to investigate their thermal stability, the influence of the oxidation state of the metal on the growth of films, the incorporation of nitrogen or fluorine, and the dependence of the preferential orientation of the films.

Experimental Section

The precursors were synthesized as described below. The melting points were measured in open capillary tubes using a Buechi 510 instrument. The ^{1}H NMR and ^{19}F NMR spectra were recorded on a Bruker AC 200P instrument. Electron-impact mass spectra were obtained from a VG Tritech Tribid mass spectrometer (mass resolution ($m/\Delta m$) = 1000; ionizing energy = 70 eV; ion source potential = +4 kV; ion source temperature = 180 °C; probe temperature = 150–250 °C; source pressure = 10^{-5} mbar; analyzer pressure = 10^{-7} mbar). The infrared spectra were measured on a Perkin-Elmer 883 infrared spectrometer with RbJ disks in the 4000–200-cm^{-1} region.

The samples were investigated in a Mettler TA-2000C thermoanalyzer at a heating rate of 10 K min^{-1}. The atmosphere was either air or argon. In pyrolysis experiments the samples were filled in a ceramic vessel and heated in an oven under an atmosphere of air. After being heated, the residuals were analyzed by X-ray diffraction (XRD).

The chemicals were purchased from Fluka in the highest purity available. The ligands H(thd) (2,2,6,6-tetramethyl-3,5-heptanedione) and H(fdh) (6,6,6-trifluoro-2,2-dimethyl-3,5-hexanedione) were synthesized via Claisen condensation (NaH suspension in dimethoxyethane). The crude products were precipitated with copper acetate,[16] recrystallized in ethanol, and stored as copper salts. Small amounts were hydrolyzed and distilled before preparing the lanthanide complexes.

Synthesis. (*A*) *Synthesis of $Ce^{IV}L_4$.* The syntheses of the complexes were carried out in open glass vessels using a 50% ethanolic solution of $CeCl_3(H_2O)_7$ (1.49 g, 4 mmol in 50 mL). A second solution was prepared containing 2.9 equiv (H(thd) = 2.14 g; H(fdh) = 2.28 g; 11.6 mmol) of the ligand, the appropriate amount of 4 M aqueous NaOH (2.9 mL), and 50 mL 95% ethanol as solvent. The latter solution was slowly added to the cerium chloride containing solution under stirring. The crude products were filtered through a fritte (medium porosity) and dried under reduced pressure.

(*B*) *Synthesis of $Ce^{III}L_3$phen.* The procedure was that described in A except for the addition of 1.1 equiv of 1,10-*o*-phenanthroline (phen, 0.87 g, 4.4 mmol) to the ethanolic cerium solution to obtain the adducts Ce(thd)$_3$phen and Ce(fdh)$_3$phen.

Tetrakis[2,2,6,6-tetramethyl-3,5-heptanedionato]cerium (Ce(thd)$_4$). The compound was synthesized by method A. The crude product sublimed at 180 °C/0.1 Torr. The product was obtained as a dark brown-red powder. The yield was 80%. The solubility at room temperature in the common organic solvents is excellent. No melting was observed up to 270 °C. Anal. Calcd for $C_{44}CeH_{76}O_8$: C, 60.52; H, 8.77. Found: C, 60.60; H, 8.77. NMR in $CDCl_3$/TMS: δ (^{1}H) 1.11 [s, 18 H, ^{t}Bu], 5.33 (s, 1 H, C(=O)CHC(—O)] ppm. NMR in acetone-d_6/TMS: δ (^{1}H) 1.14 [s, 18 H, ^{t}Bu], 5.62 [s, 1 H, C(=O)CHC(—O)] ppm. IR (RbJ) 2962, 2869, 1589, 1564, 1544, 1502, 1399, 1386, 1358, 1246, 1225, 1174, 1140, 963, 869, 793, 758, 734, 603, 481, 410, 220 cm^{-1}.

Tetrakis[6,6,6-trifluoro-2,2-dimethyl-3,5-hexanedionato]-cerium Ce(fdh)$_4$. The compound was synthesized by method A. The crude product was an oil which solidified after stirring the reaction mixture for about 1 week. After sublimation (140 °C/0.1 Torr), the product was obtained as a dark brown-red powder (mp = 123–127 °C). The yield was 78%. The solubility at room temperature in the common organic solvents is excellent. Anal. Calcd for $C_{32}CeF_{12}H_{40}O_8$: C, 41.47; H, 4.38. Found: C, 41.41; H, 4.32. NMR in $CDCl_3$/TMS and external standard $CFCl_3$: δ (^{1}H) 1.18 [s, 9 H, ^{t}Bu], 5.95 [s, 1 H, C(=O)CHC(—O)]; δ (^{19}F) –75.60 [s, CF_3] ppm. IR (RbJ) 2973, 2936, 1617, 1594, 1547, 1517, 1479, 1452, 1429, 1395, 1366, 1306, 1250, 1225, 1193, 1152, 1116, 956, 850, 805, 688, 573, 521, 466, 397, 220 cm^{-1}.

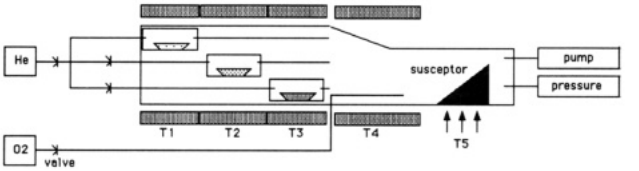

Figure 1. Schematic representation of the horizontal MOCVD apparatus.

Table I. Typical Growth Parameters for the Four Cerium Precursors[a]

	Ce(thd)$_4$	Ce(thd)$_3$phen	Ce(fdh)$_4$	Ce(fdh)$_3$phen
evap temp, °C	170–205	180–220	120–140	180–220
oxygen flow, sccm	0–108	0–180	0–144	0–180
substrate temp, °C	300–500	400–550	250–600	275–550

[a] For all: substrate, Si[100], quartz; pressure, 17–25 mbar; helium flow, 66 sccm.

1,10-Phenanthrolinetris[2,2,6,6-tetramethyl-3,5-heptanedionato]cerium (Ce(thd)$_3$phen). The compound was synthesized by method B. The complex was a brown-colored solid after sublimation (200 °C/0.1 Torr) and the yield was 75%. At room temperature the compound is soluble in organic solvents such as acetone and chloroform but only slightly soluble in hexane. The complex decomposed in air within a few weeks. Anal. Calcd for $C_{45}CeH_{65}N_2O_6$: C, 61.12; H, 7.53; N, 3.22. Found: C, 61.86; H, 7.20; N, 3.23. NMR in acetone-d_6/TMS: δ (^{1}H) 1.70 [s, 54 H, ^{t}Bu], 12.47 [s, 3 H, C(=O)CHC(—O)], 7.57 [d, 2 H J = 8 Hz, Ar C–H], 7.26 [s, 2 H, Ar C–H], 5.15 [d, 2 H, J = 8 Hz, Ar C–H], –4.70 [s, 2 H, Ar C–H] ppm. IR (RbJ) 2961, 2902, 2865, 1570, 1534, 1502, 1449, 1413, 1358, 1226, 1181, 1137, 791, 758, 728, 719, 600, 473, 405 cm^{-1}.

1,10-Phenanthrolinetris[6,6,6-trifluoro-2,2-dimethyl-3,5-hexanedionato]cerium (Ce(fdh)$_3$phen). The compound was synthesized by method B. The complex was a yellow solid after sublimation (170 °C/0.1 Torr), and the yield was 87% (mp = 185–190 °C). At room temperature the compound is soluble in organic solvents such as acetone and chloroform but only slightly soluble in hexane. Anal. Calcd for $C_{36}CeF_9H_{38}N_2O_6$: C, 47.47; H, 4.23; N, 3.09. Found: C, 47.87; H, 4.24; N, 3.33. NMR in $CDCl_3$/TMS and external standard $CFCl_3$: δ (^{1}H) 1.55 [s, 27 H, ^{t}Bu], 11.96 [s, 3 H, C(=O)CHC(—O)], 7.31 [d, 2 H, J = 8 Hz, Ar C–H], 6.71 [s, 2 H, Ar C–H], 5.86 [d, 2 H, J = 8 Hz, Ar C–H], –1.09 [s, 2 H, Ar C–H]; δ (^{19}F) –75.60 [s, CF_3] ppm. NMR in acetone-d_6/TMS and external standard $CFCl_3$: δ (^{1}H) 2.10 [s, 27 H, ^{t}Bu], 12.67 [s, 3 H, C(=O)CHC(—O)], 7.02 [d, 2 H, J = 8 Hz, Ar C–H], 6.48 [s, 2 H, Ar C–H], 5.48 [d, 2 H, J = 8 Hz, Ar C–H], –0.30 [s, 2 H, Ar C–H]; δ (^{19}F) –73.44 [s, CF_3] ppm. IR (RbJ) 2970, 2907, 2873, 1619, 1592, 1541, 1513, 1470, 1427, 1393, 1368, 1349, 1301, 1251, 1223, 1184, 1160, 1137, 1109, 952, 932, 863, 846, 796, 767, 729, 722, 688, 568, 478, 392 cm^{-1}.

Film Deposition. The growth experiments were carried out in the horizontal quartz MOCVD system described elsewhere.[14] A schematic representation of the cold wall reactor is shown in Figure 1. In Table I typical growth parameters are given for the four different precursors. In every experiment 20–200 mg of the precursors was used. The total time of deposition was varied between 20 and 90 min to realize film thicknesses in the range of 300–3000 Å. After deposition, the substrates were immediately removed from the reactor and cooled to room temperature in air. The evaporation rate was determined by weight loss of the ceramic boat that was used as an evaporator.

For Ce(thd)$_4$ all experiments were carried out with helium or a mixture of helium and H(thd) as carrier gas. In the latter case helium was bubbled through the liquid ligand at room temperature before placing it into the evaporation chamber.

(16) Hammond, G. S.; Nonhebel, D. C.; Wu, C. S. *Inorg. Chem.* **1963**, *2*, 72.

(17) McCrackin, F. L.; Passaglia, E.; Stromberg, R. R.; Steinberg, H. L. *J. Res. Natl. Bur. Stand.* **1963**, *67A*, 363.

Table II. Mass Spectra[a] of Ce(fdh)$_4$ and Ce(fdh)$_3$phen and the Values from the Literature for Ce(fdh)$_4$

fragments[b]	Ce(fdh)$_4$, lit.[c] *m/z* and (RA[d])	Ce(fdh)$_4$ *m/z* and (RA[d])	Ce(fdh)$_3$phen *m/z* and (RA[d])
$[CeL_4]^+$	920 (8.7)	920 (1.2)	
$[CeL_4 - F]^+$	901 (1.7)		
$[CeL_3phen]^+$	*e*	*e*	905 (45.5)
$[CeL_3]^+$	725 (100)	725 (100)	725 (100)
$[CeL_2phen]^+$	*e*	*e*	710 (140.9)
$[CeL_2F]^+$	549 (2.5)	*f*	*f*
$[CeL_2]^+$	530 (29.4)	530 (140)	530 (131.5)
$[CeL_2 - CO]^+$	502 (5)	502 (10.3)	502 (12.4)
$[CeL_2F - CF_3]^+$	480 (7.2)	480 (25.9)	480 (30.6)
$[CeL_2 - CO - C_4H_9F]^+$	426 (4.6)	426 (14.5)	426 (140)
$[CeLF]^+$	354 (20.3)	354 (66.9)	354 (7.1)
$[CeLF - CO]^+$	326 (6.4)	326 (16)	326 (19.5)
$[CeLF_2 - CF_3]^+$	304 (18.6)	304 (60.5)	304 (50.7)
$[CeF_2]^+$	178 (7.9)	178 (22.8)	178 (16.8)

[a] All masses are nominal masses. [b] L = fdh. [c] Parameters of the mass spectrometer: ionizing energy of 70 eV, ion repeller potential of 2.2 V, ion-source temperature of 60–90 °C, and probe temperature of 140–190 °C. [d] RA = relative abundance in percent. [e] Fragment not possible. Fragment not observed.

The thicknesses of the films were determined by profilometry and ellipsometry. A small area of the substrates was covered by a platinum foil during deposition. The step distance between substrate and film was measured with a Tencor alpha-step 200 profilometer. The films were also investigated by a Plasmos SD2300 ellipsometer. The reflection of ellipsometric polarized light of a He laser (λ = 632.8 nm) was used to determine the thickness and the real refractive index of the films. The basic assumptions for the refinement of these two parameters were that the films were nonabsorbing and isotropic and that the single-layer model is valid.[17] The two independent measurements of the thicknesses, each having an error of 10%, yielded results with differences of about 10%. These thicknesses were used to calculate the growth rate (G) of the films.

UV–vis absorption spectra of some films on quartz were measured on a Uvikon 941 spectrophotometer.

The fluorine, carbon and nitrogen contents of the films were determined by wavelength-dispersive X-ray spectroscopy (WDX) using a Cameca SX50 and by Auger emission spectroscopy (AES) using a Perkin-Elmer 4300 scanning Auger microscope. The topology of the films were studied by scanning electron microscope (SEM) using a Cambridge S630 and atomic force microscope (AFM) using a Topometrix TMX 2000. A Phillips PW1710 powder X-ray diffractometer with the typical Bragg–Brentano geometry was used to check the phases and the preferential orientations that are present in the films.

Results and Discussion

Mass Spectrometry. Ions containing cerium were identified by the two isotopes ^{140}Ce and ^{142}Ce with a ratio of 8:1.

The results from the experiments of the fluorinated fdh complexes and the corresponding data from the literature are listed in Table II. The results for the nonfluorinated thd compounds and the data found in the literature for ^{139}La(thd)$_3$[18] are given in TableIII. The data from the literature were used to assign the *m/z* signals of our MS results. The fragmentation patterns obtained in this way were analogous to those reported in the literature. To compare the RA (relative abundance) of the different compounds within one table, the values of the fragment $[CeL_3]^+$ in Table II and $[ML_2]^+$ in Table III was set to 100%. Peaks with $m/z < 180$ have not been considered due to the superposition of the fragments from free ligands.

Table III. Mass Spectra[a] of Ce(thd)$_4$ and Ce(thd)$_3$phen and the Values from the Literature for ^{139}La(thd)$_3$

fragment[b]	M = ^{139}La[c] RA[d]	M = Ce Ce(thd)$_4$ *m/z* and (RA[d])	M = Ce Ce(thd)$_3$phen *m/z* and (RA[d])
$[ML_4]^+$		873 (0.8)	
$[ML_3phen]^+$			869 (0.2)
$[ML_3]^+$	20	689 (173)	689 (81.8)
$[ML_3 - C_4H_9]^+$	40		632 (1)
$[ML_3 - C_4H_9]^{2+}$	1	316.1 (3.8)	
$[ML_3 - C_4H_9 - CH_3]^{2+}$	2		308.4 (3)
$[ML_3 - 2C_4H_9]^+$	6	287 (9.9)	287 (3.5)
$[ML_2]^+$	100	506 (100)	506 (100)
$[ML_2 - 2CH_3]^+$	4	491 (1.4)	491 (2)
$[ML]^+$	1	323 (0.7)	323 (1.5)

[a] All masses are nominal masses. [b] L = thd. [c] Literature: time-off-flight mass spectrometer. [d] RA = relative abundance in percent.

The main result, as can be seen from the data in Tables II and III, is the appearance of analogous fragments with similar intensities at *m/z* below $[ML_3]^+$ for all the compounds in the different oxidation states. Consequently the fragmentation mechanisms must be the same for cerium(III) and cerium(IV) in this range. This can be explained by an intramolecular reduction of cerium(IV) to cerium(III) (step 2), after the initial loss of neutral radical L$^\bullet$, as first described by Shannon et al.[19] (step 1):

$$[Ce(IV)L_4]^{\bullet+} \rightarrow L^\bullet + [Ce(IV)L_3]^+ \quad \text{(step 1)}$$

$$[Ce(IV)L_3]^+ \rightarrow [Ce(III)L_3]^{\bullet+} \quad \text{(step 2)}$$

$$[Ce(III)L_3]^+ \rightarrow [Ce(III)L_2]^{\bullet+} + L^\bullet \quad \text{(step 3)}$$

The following step (step 3), another loss of L$^\bullet$, can be observed for all the lanthanide complexes. In the fluorinated compounds the low or undetectable abundance of the odd-electron molecular ion $[CeL_4]^{\bullet+}$ is explained by rapid loss of L$^\bullet$.

The tendency to form metal–fluorine species (see Table II) is well documented by our data. The formation of such fragments is only possible by fluorine migration from ligand to metal, which is favoured by the hard-acid character of cerium.[20]

The adducts CeL$_3$phen show different intensities for their fragments containing phen which are detectable in a reasonable range only for the fluorinated compounds. From this, the removal of phen is easier in the nonfluorinated compound. The bonding of phen to the metal center in the adducts is a Lewis base/Lewis acid interaction. The electron-withdrawing CF_3 group in the ligand reduces the relative electron density at the metal center. Thus, the Lewis acid character of the metal center is increased and a stronger interaction with the Lewis base phen occurs. This interaction is weaker in the nonfluorinated compound, thereby explaining the absence of fragments containing phen.

Infrared Spectroscopy. The results are summarized in Table IV.

The C=O and C=C stretching vibrations for all the compounds occur in the range of 1500–1650 cm^{-1} as two strong bands and were assigned as described in the

(18) McDonald, J. D.; Maegrave, J. L. *J. Less-Common Met.* **1968**, *14*, 236.

(19) Shannon, J. S.; Swan, J. M. *Chem. Commun.* **1965**, *1*, 33.

(20) Schildcrout, S. M. *Inorg. Chem.* **1985**, *24*, 760.

Table IV: Infrared Spectroscopic Data[a] of $Ce(thd)_4$, $Ce(fdh)_4$, $Ce(thd)_3phen$, and $Ce(fdh)_3phen$

substance	(C=O) str[b]	(C=C) str	(CF_3) str	(M–O) str
$Ce(thd)_4$	1564 vs 1542 vs	1500 s		410 w
$Ce(fdh)_4$	1593 vs	1517 s	1306 vs	397 w
$Ce(thd)_3phen$	1571 s	1503 s		405 w
$Ce(fdh)_3phen$	1619 vs	1513 s	1303 vs 1137 vs	392 w

[a] vs = very strong, s = strong, m = medium, w = weak, and vw = very weak; the experimental error was in the range of ±2 cm^{-1}. [b] str = stretching mode.

literature.[21,22] However, for $Ce(thd)_4$ a definitive assignment is not possible since three strong bands were observed in this region.

Comparing the results for the fluorinated (ligand = fdh) with those for the nonfluorinated compound (ligand = thd), one observes a clear tendency for the (C=O) and (C=C) stretching vibrations to shift to higher frequencies and for the (M–O) stretching vibration to shift to lower frequencies in the fdh complexes. Liang et al.[23] observed similar shifts with Eu(III) complexes of the fluorinated ligand tfa (H(tfa) = 1,1,1-trifluoro-2,4-pentanedione). Generally the electron-withdrawing effect of the fluoroalkyl α-substituent is responsible for this shift.

The influence of the oxidation state on the band position of the carbonyl groups is clear: the bands of Ce(III) are shifted to higher frequencies as compared to those of Ce(IV). Therefore, the double-bond character of the carbon–oxygen bond is reduced in Ce(IV). The charge-to-radius ratio may explain this observation. Clearly the ratio of Ce(IV) is larger than that of Ce(III), i.e., 4.3/Å and 2.9/Å, respectively. Assuming only ionic forces between the metal center and the oxygen atom in the complexes, the "metal–oxygen bond" is stronger in Ce(IV) and the corresponding carbon–oxygen double bond is weaker. An analogous discussion was published by Sievers et al.[24] for various hfa (H(hfa) = 1,1,1,5,5,5-hexafluoro-2,4-pentanedione) compounds.

However, a sequence of decreasing double-bond character in the carbon–oxygen bond could be obtained:

$$Ce(fdh)_3phen > Ce(fdh)_4 > Ce(thd)_3phen > Ce(thd)_4$$

Comparing the data of the M–O stretching frequencies, there are only small differences. Assuming no superposition with other vibrations and taking into consideration an experimental error of about 2 cm^{-1}, a sequence of decreasing M–O bond strength is obtained, which is inverse to that described above. Again this sequence can be explained by the influence of fluorination and charge to radius ratio. Fluorine groups weaken the M–O bond and a high charge-to-radius ratio strengthens it.

Thermal Analysis. Figure 2, parts a and b, show the results of the TGA (thermogravimetric analysis) of all the precursors in argon and air, respectively. In Figure 2c,d the results of the DTA (differential thermal analysis) and TGA are illustrated for $Ce(thd)_4$ in air and $Ce(fdh)_4$ in argon, respectively, and are representative results for the measurements in different atmospheres.

The sharp endothermic peaks in the DTA curves (marked with an asterix in Figure 2c,d) were identified as the melting of the sample. In a separate run, where just after this endothermal peak the temperature program was changed from dynamic heating to dynamic cooling, the exothermal peak arising from the crystallization of the melt was observed. All the investigated precursors melt in the same range as vaporization starts. The results are all summarized in Table V.

Measurements in air for all the samples excluding $Ce(fdh)_4$ revealed a large exothermic peak (see Figure 2c) and a weight loss of only 79–84% (see Figure 2b). The exothermic peak (noted in Table V as T_{exo}) is in the same range as $T_{1/2}$ (see Table V). The exothermal reaction of the reactant with air takes place during evaporation. The XRD analysis of the residue in case of $Ce(thd)_4$ showed the presence of single phase cerium dioxide.

For the experiments carried out under argon the weight loss was in the range of 90–97% (see Figure 2a). The evaporation of the reactant is not influenced by the reaction of the vapor and the decomposition products with air. No exothermal effects were observed on the DTA curves. The $T_{1/2}$ values are shifted up to a higher temperature from 34 °C ($Ce(fdh)_4$) to 68 °C ($Ce(thd)_3phen$).

Comparing the values of $T_{1/2}$ (in argon) the following sequence of decreasing volatility can be stated: $Ce(fdh)_4 \gg Ce(thd)_4 \gg Ce(fdh)_3phen > Ce(thd)_3phen$. The crystal structures of several β-diketonato-complexes show the distorted square antiprismatic stereochemistry.[25] The metal center is surrounded by the ligands to form an almost spherical molecule. The nonpolar CF_3 groups in the fdh complex reduces intermolecular interactions and, therefore, $Ce(fdh)_4$ is the most volatile precursor. Although, the lanthanide(III) adducts have the same distorted square antiprismatic stereochemistry (lanthanide = europium[26]) they are less volatile than the cerium(IV) complexes. The coordination of the nitrogen atoms of phen to the metal center results in a distorted distribution of charge in the complexes. This distortion destroys the spherical symmetry of the molecule which is essential for high volatility, and thus the influence of fluorination is reduced.

Pyrolysis of the Fluorinated Precursors. The conditions of the heating process and the results are listed in Table VI.

The samples heated at 300 °C were amorphous, and only the precursor itself was identified by infrared spectroscopy.

The results of the experiments at higher temperatures show no differences between the Ce(III) and Ce(IV) precursor. Considering the redox potential of $E_0^{Ce^{IV}/Ce^{III}} = 1.443$ V, there is a clear tendency for reduction from Ce(IV) in the precursor to Ce(III) in the fluoride. The formation of CeF_3 occurs via migration of the fluorine from the ligand to cerium. Another oxidation step occurs on going to higher temperatures or longer heating times, whereby CeF_3 is converted into CeO_2.

Cunningham et al.[27] described equivalent results on heating cerium fluoride in air. Pure cerium dioxide was obtained at 600 °C.

(21) Pinchas, S.; Silver, B. S.; Laulicht, I. *J. Chem. Phys.* **1967**, *46*, 1506.
(22) Nakamoto, K.; Behnke, G. T. *Inorg. Chem.* **1967**, *6*, 433.
(23) Liang, C. Y.; Schimitschek, E. J.; Trias, J. A. *J. Inorg. Nucl. Chem.* **1970**, *32*, 811.
(24) Morris, M. L.; Moshier, R. W.; Sievers, R. E. *Inorg. Chem.* **1963**, *2*, 411.
(25) Kepert, D. L.; Patrick, J. M.; White, A. H. *J. Chem. Soc., Dalton Trans.* **1983**, 567.
(26) Jian, Y.; Xian-Qi, H.; Zhong-Yuan, Z.; Li, L. *J. Struct. Chem.* **1989**, *8*, 187.
(27) Cunningham, B. B.; Feay, D. C.; Pollier, M. A. *J. Am. Chem. Soc.* **1954**, *76*, 3361.

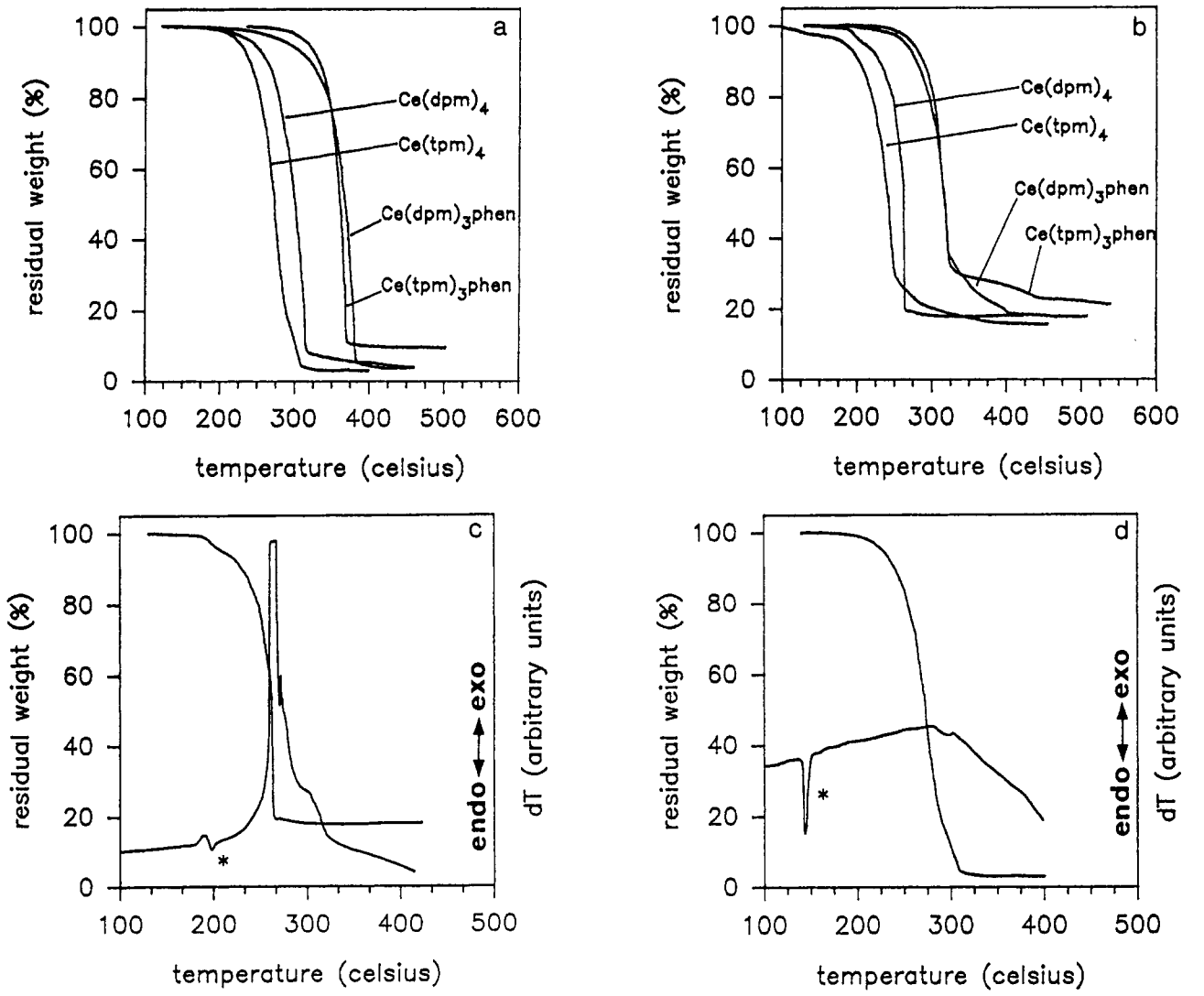

Figure 2. TGA measurements in argon (1a) and air (1b), respectively. TGA/DTA results of $Ce(thd)_4$ in air (1c) and $Ce(fdh)_4$ in argon (1d) as representative examples for all other precursors.

Table V. DTA/TG Measurements of the Cerium Compounds in Air and Argon with a Heating Rate of 10 K min^{-1}

compound	mp, °C	$T_{1/2}$,[a] °C	residual, %	T_{exo},[b] °C	atm[c]
$Ce(thd)_4$	199	270	18	265	air
$Ce(thd)_3phen$	211	306	18	293	air
$Ce(fdh)_4$	140	243	15.9	243 (vs)	air
$Ce(fdh)_3phen$	195	318	21	309 (s)	air
$Ce(thd)_4$	200	312	4		Ar
$Ce(thd)_3phen$	205	374	3.8		Ar
$Ce(fdh)_4$	143	277	3.1		Ar
$Ce(fdh)_3phen$	195	362	9.5		Ar

[a] $T_{1/2}$ = temperature were the wheight loss of the sample is 50%. [b] Maximum of the first exothermal peak; s = small and vs very small. [c] atm = atmosphere in the oven.

Film Deposition and Analysis. Figure 3 shows the logarithmic plot of the evaporation rate for all four precursors. The volatility of these precursors can be clearly distinguished: $Ce(fdh)_4 \gg Ce(thd)_4 > Ce(fdh)_3phen \approx Ce(thd)_3phen$, and this order agrees well with the results of the thermal analysis.

No improvement of the evaporation rate of $Ce(thd)_4$ was found for the carrier gas mixture helium/H(thd).

The growth rate G as a function of the precursor evaporation rate, oxygen flow and substrate temperature is shown in Figure 4–6 and the details of these experiments are listed in Table VII.

Table VI. Pyrolyses of $Ce(fdh)_4$ and $Ce(fdh)_3phen$ in Air

precursor	temp, °C	time, h	results of XRD
$Ce(fdh)_4/Ce(fdh)_3phen$	300	1	amorphous
$Ce(fdh)_4/Ce(fdh)_3phen$	470	1	CeF_3
$Ce(fdh)_4/Ce(fdh)_3phen$	470	12	CeF_3 and CeO_2
$Ce(fdh)_4/Ce(fdh)_3phen$	1000	3	CeO_2

Figure 4 shows the dependence of G on the evaporation rate. There is an evident difference between the nonfluorinated (Figure 4a) and the fluorinated precursors (Figure 4b): G with the latter compounds saturating at a low level, whereas G for the former compounds increases linearly with an increasing evaporation rate. The linear increase can be explained by mass-flow controlled growth of the films, and the saturation must be explained by a different limiting factor that is not varied in this experiment.

Variation of the oxygen flow is shown in Figure 5. In this figure saturation can be found for nonfluorinated compounds and linear increase for fluorinated compounds. Therefore, the oxygen flow controls the growth rate for fluorinated cerium precursors.

It is remarkable that there is no significant difference in the growth characteristics for Ce(III) and Ce(IV) complexes with the same ligands.

There exists a clear difference between the growth rates for $Ce(thd)_4$ as a function of carrier gas. At low oxygen

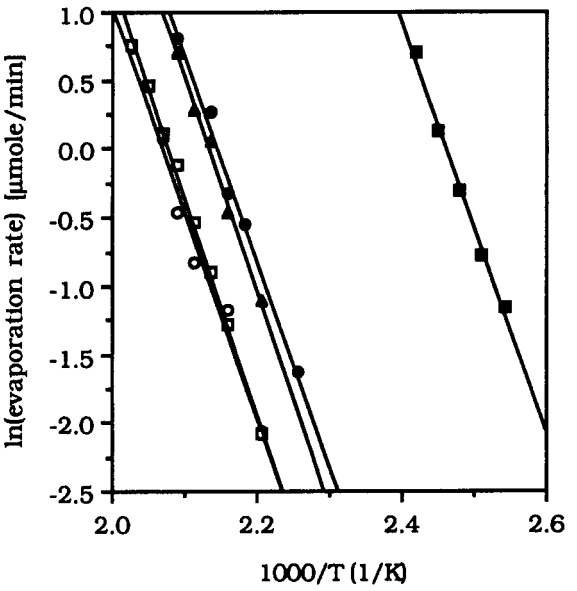

Figure 3. Evaporation rate of $Ce(thd)_4$ with helium as carrier gas (full circle), $Ce(thd)_4$ with helium/H(thd) as carrier gas (full triangular), $Ce(thd)_3phen$ (empty circle), $Ce(fdh)_4$ (full square), and $Ce(fdh)_3phen$ (empty square).

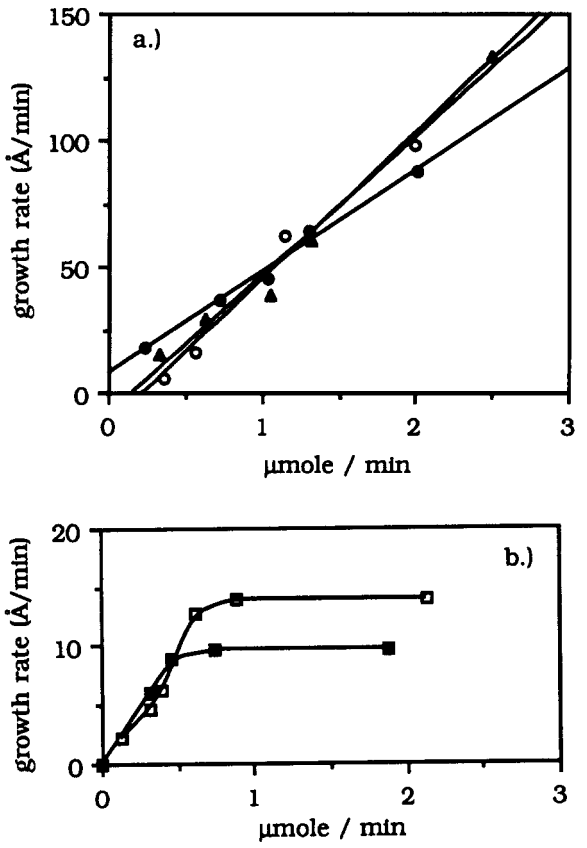

Figure 4. (a) Growth rate as a function of evaporation rate for $Ce(thd)_4$ with helium as carrier gas (full circle), $Ce(thd)_4$ with helium/H(thd) as carrier gas (full triangular), $Ce(thd)_3phen$ (empty circle). (b) Growth rate as a function of evaporation rate for $Ce(fdh)_4$ with (full square) and $Ce(fdh)_3phen$ (empty square).

flows the growth is significantly slower for He/H(thd) and without any oxygen there is even no film growth observable. At high oxygen flows the growth rates for He and He/H(thd) as carrier gas become almost equal. This difference can be explained by thermal stabilization of $Ce(thd)_4$ in the gas phase by H(thd).

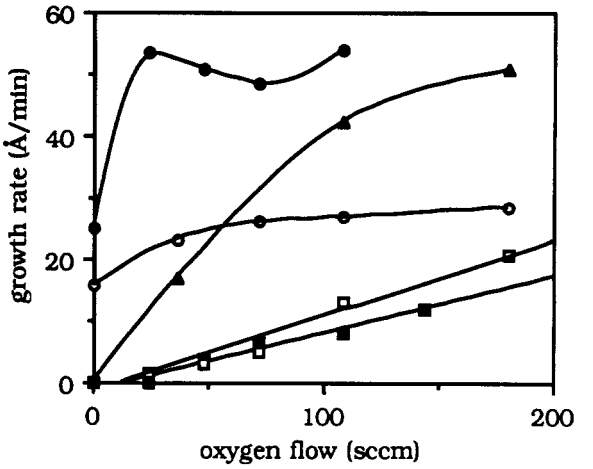

Figure 5. Growth rate as a function of the oxygen flow. $Ce(thd)_4$ with helium as carrier gas (full circle), $Ce(thd)_4$ with helium/H(thd) as carrier gas (full triangular), $Ce(thd)_3phen$ (empty circle), $Ce(fdh)_4$ (full square), and $Ce(fdh)_3phen$ (empty square). All evaporation rates were in the range of 1.2 μmol/min, except 0.6 μmol/min was used for $Ce(fdh)_4$.

The growth rate as a function of the substrate temperature is shown in Figure 6a. Initially, $Ce(thd)_3phen$ was investigated only for substrate temperatures higher than 400 °C. Experiments carried out later failed because the compound decomposed in air. Thus, no full data set was available for this precursor for Figure 6a. The features for all interpolated curves of the three other compounds are the same. There is a starting temperature of film growth and G increases sharply by increasing the temperature above this starting point. In this range the growth mechanism can be regarded as kinetically controlled. Then G reaches a top level, which is determined by the mass flow of the precursor or oxygen. Above a critical temperature G decreases due to thermal decomposition of the precursor before reaching the substrate.[14] This decomposition temperature depends strongly on the MOCVD system used and on the precursor. Nevertheless, it can be used as a guide to the thermal stability of each precursor. This leads to the following order of thermal stabilities in this MOCVD system:

$$Ce(thd)_4 > Ce(fdh)_4 > Ce(fdh)_3phen$$

The stabilization of $Ce(thd)_4$ in the experiments using a mixture of He and H(thd) as a carrier gas can be clearly seen in Figure 6b in the high temperature range ($1000/T < 2.5$). This method was first used in gas chromatographic experiments[28] and then in growth experiments of $YBa_2Cu_3O_{4-y}$ for the stabilization of $Ba(thd)_2$.[29] The previously reported results for the growth rate of $Ce(thd)_4$ + H(thd)[14] showed an unusual step function of G. This feature was an artifact of the ellipsometric refinement, and the corrected values are presented here.

It is interesting to note that the order of thermal stabilities are in good agreement with the results of the IR study on the M–O bond strengths. The thermal stability decreases with decreasing M–O bond strength. In addition, the low intensity of the molecular ion in the MS study suggests a stepwise removal of the ligands thd, fdh, or phen for the first fragmentation. In the case of

(28) Matsubara, N.; Kuwamoto, T. *Anal. Chim. Acta* **1984**, *161*, 101.
(29) Dickinson, P. H.; Geballe, T. H.; Sanjurjo, D.; Hildenbrand, D.; Craig, G.; Zisk, M.; Collman, J.; Banning, S. E.; Sievers, R. E. *J. Appl. Phys.* **1989**, *66*, 444.

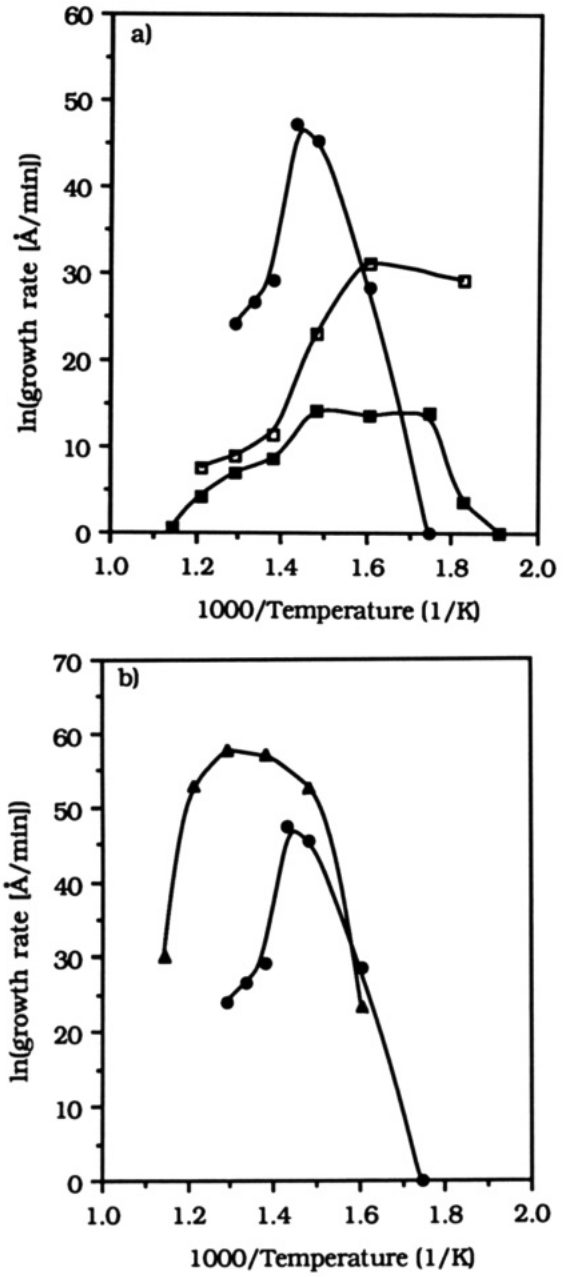

Figure 6. (a) Growth rate for $Ce(thd)_4$ with helium as carrier gas (full circle), $Ce(fdh)_4$ (full square), and $Ce(fdh)_3$phen (empty square). All evaporation rates were in the range of 1.2 μmol/min except 0.6 μmol/min was used for $Ce(fdh)_4$. (b) Growth rate for $Ce(thd)_4$ using helium (full circle) or helium/H(thd) (empty circle) as carrier gas.

Table VII. Growth Parameters for the Experiments Shown in Figures 3–5 (Fixed Means That It Was a Fixed Value for Each Precursor but Not the Same for All Precursors)

	Figure		
	4	5	6
evap temp	variable	fixed	fixed
oxygen flow, sccm	108	variable	108
substrate temp, °C	450	fixed 450/500	variable

$Ce(thd)_4$ an equilibrium can be proposed in the following way:

$$Ce(thd)_4 \rightleftharpoons Ce(thd)_3 + thd^*$$

The addition of free ligand shifts the equilibrium to the left side. This could be a possible explanation for the stabilization of H(thd).

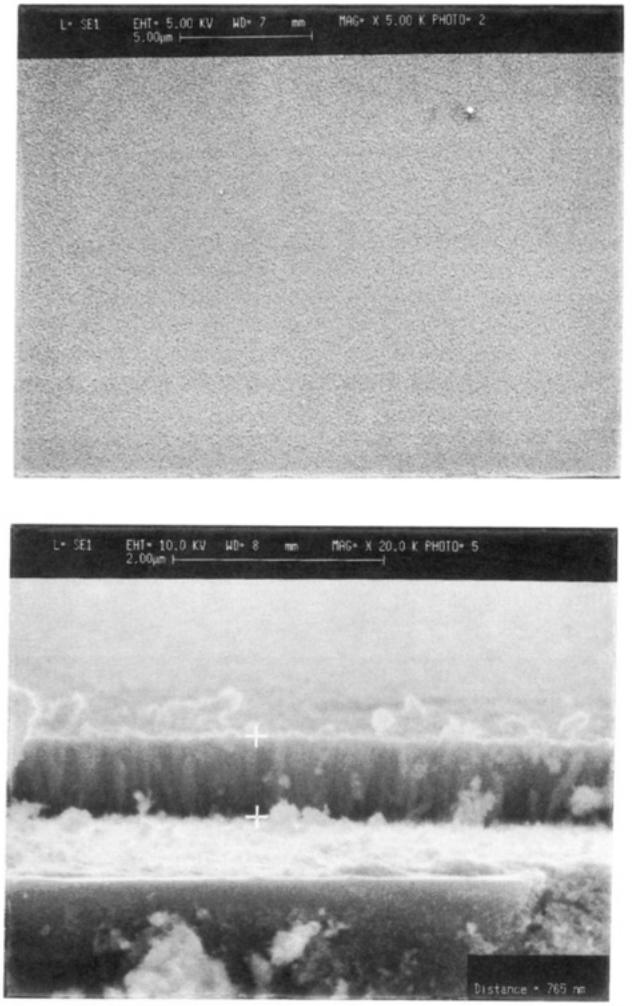

Figure 7. SEM pictures of a CeO_2 film on Si[100] using $Ce(thd)_4$ as precursor and a substrate temperature of 450 °C: (a, top) top surface; (b, bottom) cross section.

For all films that showed any crystalline phase all reflections in the XRD patterns could be explained by CeO_2. For $Ce(thd)_4$, $Ce(thd)_3$phen, and $Ce(fdh)_3$phen no significant reflections could be observed for substrate temperatures below 400 and above 500 °C; however, between these temperatures CeO_2 was found with a strong preferential orientation in [100] direction. The films grown with $Ce(fdh)_4$ are an exception to these results. At a substrate temperature of 300 °C the CeO_2 film grew in the [111] direction, and by increasing the substrate temperature the preferential order became poorer. From the reflections of the XRD pattern of the CeO_2 films a cubic lattice constant of $a = 5.40$ (2) Å can be determined in good agreement with the value of 5.41 Å of the JCPDS card.[30] Also typical grain sizes of about 500–1000 Å can be calculated by using the Scherrer formula.[31]

The films were transparent, very smooth and homogeneous as could be proved by profilometry, ellipsometry and WDX. Figure 7 shows a scanning electron microscopy (SEM) picture of a typical CeO_2 film which was grown with $Ce(thd)_4$ as precursor. The morphology of this film

(30) Powder Diffraction File, Card No 39-1390, Joint Committee on Powder Diffraction Standard, Swarthmore, PA.

(31) (a) Scherrer, P. *Göttinger Nachrichten* **1918**, *2*, 98. (b) Azároff, L. V. *Elements of X-ray crystallography*; International Student Edition; McGraw-Hill: New York, 1968.

(32) Chin, T. S.; Huang, J. Y.; Perng, L. H.; Huang, T. W.; Yang, S. J.; Hsu, S. E. *Physica C* **1992**, *192*, 154.

is very similar to that observed by Chin et al. for a cerium dioxide film on Si[100].[32] As can be seen by careful inspection of the cross section, the MOCVD films of this work grow in columns. Preliminary results of AFM investigations confirm this result and yield typical diameters of these columns of several tenth of nanometers. This is comparable to the results mentioned in the Introduction.[3,4]

The AES investigations of the films yielded a surface contamination with carbon up to 20%. However, the carbon content in the films after sputtering was only 2–4%. Furthermore, the fluorine content of the films was below 2%. No nitrogen (N ≤ 1%) was found by WDX measurements in the films grown with phen adducts. The low fluorine contamination is not surprising since the pyrolysis experiments of the fluorinated precursors resulted in the oxidation of the initially produced CeF_3 to CeO_2.

Conclusion

The thermal analysis and evaporation rate experiments yielded the following decreasing order of volatility for the precursors:

$$Ce(fdh)_4 > Ce(thd)_4 > Cd(fdh)_3phen \approx Ce(thd)_3phen$$

The species which determines the growth rate is different for nonfluorinated and fluorinated compounds. For nonfluorinated compounds the precursor itself controls the growth rate. However, for fluorinated compounds the reaction gas, oxygen, plays the determining role in the growth mechanism. There was no significant difference between film growth by using Ce(III) or Ce(IV) precursors.

The dependence of the growth rate on the substrate temperature showed a decrease at high temperatures for all precursors. This decrease can be explained by gas-phase thermal decomposition of the complex. For this reason, the onset of the decrease can be regarded as a measure of thermal stability in this specific MOCVD system. Different thermal stabilities for the cerium compounds have been observed:

$$Ce(thd)_4 > Ce(fdh)_4 > Ce(fdh)_3phen$$

The IR studies yielded the same order for the strength of the metal–oxygen bond.

The use of a mixture of helium and the ligand H(thd) as a carrier gas resulted in an evident stabilization of the complex in the gas phase and in higher growth rates at elevated temperatures ($T > 500$ °C).

Cerium dioxide films with four different precursors were grown by MOCVD. The films showed a high crystallinity and a high preferential orientation for substrate temperatures in the range 400–500 °C. A low contamination with carbon was detected by AES and no nitrogen or fluorine was incorporated in the films. Even though very homogeneous and smooth films were found, it is very likely that the films consist of columns.

Acknowledgment. The research was supported by Kredite für Unterricht und Forschung, ETH Zürich, and the Swiss National Research Foundation. We would like to express our thanks to Dr. M. Maciejewski of the Institut für Technische Chemie for the DTA/TG measurements, Dr. Patscheider of the Eidgenössische Material Prüfungsanstalt for the AES measurements, Dr. Chr. Schild of the Institut für Technische Chemie. for the AFM measurements and Mr. B. Senior of I²M for the SEM measurements.